Sensors and Materials, Vol. 36, No. 6 (2024) 2391–2407
MYU Tokyo

S & M 3676

Design of Linear Motor of Electrical Nail Gun Using Magnetic Array Approach

Ming-Hung Lin,[1] Cheng-Che Yang,[2] Bo-Wun Huang,[2] Po-Hsun Chen,[1] Bing-Hong Chen,[1] Cheng-Yi Chen,[1*] and Cheng-Fu Yang[3,4**]

[1]Department of Electrical Engineering, Cheng Shiu University, Kaohsiung City, 833, Taiwan
[2]Institute of Mechatronic Engineering, Cheng Shiu University, Kaohsiung, 833, Taiwan
[3]Department of Chemical and Materials Engineering, National University of Kaohsiung, Kaohsiung 811, Taiwan
[4]Department of Aeronautical Engineering, Chaoyang University of Technology, Taichung 413, Taiwan

(Received May 7, 2024; accepted June 3, 2024)

Keywords: Halbach magnet array, electric nail gun, hybrid magnet array, Altair Flux 3D

Electric tools have become indispensable in various industries owing to their convenient portability, high energy efficiency, and capability to operate without being constrained by power cords when using batteries. Referring to the currently marketed ST-64 specification gas-powered or compressed-air-powered nail guns commonly used for concrete and steel beams, we propose a linear motor design with superior output power and operational speed for use in electric nail guns. The design process begins with designing and simulating the stator and mover of the motor using Altair Flux 3D finite element analysis software. The stator is a combination of permanent magnets and electromagnetic iron and designed to possess magnetic field properties similar to those of the Halbach magnet array. On the other hand, the mover utilizes permanent magnets with different magnetic field directions to achieve a Halbach magnet array design, resulting in a magnetic field direction opposite to that of the stator. The linear motor, formed by a combination of the stator and mover, is then analyzed and adjusted through Flux 3D finite element analysis to design a short-stroke, high-thrust linear motor leveraging the concentrated magnetic field characteristics of the magnet array. Finally, it is experimentally verified that the linear motor designed in the experiment can achieve an output force of up to an average of 90 N even when using an inferior core, reinforcing the potential and reliability of this design for practical implementation.

1. Introduction

Commonly used tools in manufacturing or machining have evolved from the initially used manual tools, upgraded to pneumatic tools in pursuit of higher work efficiency, and finally advancing to more convenient electric tools, making the operation of various industries reliant on different tools. Nail guns are a standard tool used in multiple joining applications in industries such as woodworking, construction, roofing, casting, and automotive repair. A nail gun, also

*Corresponding author: e-mail: k0464@gcloud.csu.edu.tw
**Corresponding author: e-mail: cfyang@nuk.edu.tw
https://doi.org/10.18494/SAM5131

ISSN 0914-4935 © MYU K.K.
https://myukk.org/

known as a nailer, is a handheld power tool used for fastening nails and screws. They are typically powered by compressed air or gas to drive nails or screws into surfaces such as walls, floors, and roofs. According to the descriptions in Ref. 1, traditional carpentry framing work using a handheld hammer would take approximately one minute per nail. However, opting to use a nail gun can significantly reduce the processing time for each nail to just five seconds. This change not only considerably saves on work time but also reduces the physical burden on workers. Electric tools are widely used for various functions and applications such as assembly and production lines, do-it-yourself projects, maintenance and repair, and packaging tasks. Electric tools enable more efficient handling and operation, save time, satisfy different labor requirements in various tasks, and significantly increase productivity and profitability. The development of new technologies is driving the demand for electric tools in the construction industry, making these tools more powerful, efficient, and versatile. For example, cordless electric tools are becoming increasingly popular because of their ease of use and lack of need for sockets. The advancement of the construction industry, including railways, airports, highways, commercial facilities, and housing worldwide, is increasing the demand for electric tools. Therefore, a research report in 2023 forecasted that the compound annual growth rate of the global electric tool market would be 7.2% from 2023 to 2030.[2]

Steel nails are crucial for fastening components to construction site concrete walls or metal structures. Because a significant impact energy is required, manual execution poses a considerable challenge to workers. Consequently, the predominant approach has shifted towards using pneumatic or gas-driven tools to conserve labor and reduce physical strain.[3–7] Pneumatic nail guns require a power source for compressing air from a compressor to generate kinetic energy for external output. Their primary advantages include easy accessibility to air, low operating pressure, on-site discharge of used air, and no need for pipeline recovery. However, a pneumatic tool necessitates an air pressure line to connect the compressed air source and provide power, which sometimes compromises safety in the construction environment.[4,5] It has also been noted that the noise output is another issue with pneumatic tools; such noise can be mitigated by adjusting the working pressure of the compressed air source and employing bumper materials and exhaust mufflers within the tool. On the other hand, gas nail guns utilize gas as a power source; it is ignited within the combustion chamber by a battery and drives the nail gun through combustion and explosion to complete the nailing operation.[8] This approach addresses the issues associated with pneumatic tool air pressure lines. However, it introduces new challenges, such as requiring gas canisters and ensuring gas operation safety. With the advancement of electronic technology, transitioning nail guns from pneumatic and gas-driven operation to electric operation has become a growing trend. If the power can deliver sufficient impact force, it could alleviate the problems associated with the pneumatic and gas-driven tools described above.

Reference 9 indicates that electric nail guns may suffer from insufficient power. However, after optimization, the nails can effortlessly penetrate solid teak wood. While Ref. 9 provides a schematic diagram of the electric nail gun's structure, this type of nail gun comprises multiple components, making its structure complex. When energized, the motor starts running and drives the rack to push the piston backward, compressing the spring for fixation. When the

trigger switch is pressed, the spring is released, propelling the firing pin to impact the nail and drive it into the workpiece. The overall energy conversion primarily involves converting electrical energy into mechanical energy to fire the steel nail. The structure adopted by the DCN 890 concrete nail gun of DeWalt Industrial Tool Company utilizes a flywheel as an energy storage component.[10] Firing is initiated by accelerating the flywheel to a certain speed and contacting it with the firing pin. This structure allows power to be controlled by adjusting the flywheel speed. When not in use, the flywheel stops, eliminating the risk of accidental firing due to lack of power. However, one has to wait for the motor to store energy in the flywheel, resulting in a lower construction speed. Wang *et al.* discussed the use of linear voice coil motors to drive the nail ejection device, aiming to address the issue of bulky nail gun size.[11] Through a power amplification mechanism, they were able to complete thrust tests. Chen *et al.* discussed the application of electromagnets in electromagnetic suction cups for lifting heavy objects.[12] They utilized magnetic yokes and poles to direct the electromagnetic effect generated by the coil to the suction surface for object adhesion. The results of these analyses collectively suggest the potential for further enhancement of impact energy in electric nail guns.

The Halbach magnet array is a magnetic arrangement method commonly used to enhance magnetic fields. The German physicist Klaus Halbach proposed it in the 1970s.[13] Its characteristic feature involves arranging a series of permanent magnets on a plane, with their directions and strengths precisely designed and controlled to generate a strong magnetic field. Unlike traditional magnet layout methods, the magnetic field of the Halbach magnet array is not uniformly distributed throughout the layout. Instead, it is enhanced in specific areas and weakened in others.[14–20] The Halbach magnet array can also concentrate the magnetic field on one side. Besides the benefits of enhanced magnetic force, the reduced magnetic force at the back can minimize interference with other parts, thus reducing the need for magnetic shielding materials and offering linear motor functionality for low-frequency electromagnetic operation. Therefore, in this study, we will refer to the principles of the Halbach magnet array and utilize Altair Flux 3D magnetic finite element analysis software to simulate, analyze, and design the stator and mover of the motor. We aim to devise a linear motor design with a concentrated magnetic field provided by the magnet array and strong thrust with a short stroke, thereby achieving a linear motor that can act as the power source for an electrical nail gun.

2. Linear Motor Design and 3D Magnetic Field Finite Element Analysis

2.1 Linear motor design

The conceptual design of the linear motor proposed in this paper is illustrated in Fig. 1. The magnet array technique is utilized to form the concentrated magnetic fields on one side to achieve the design of linear motors while maintaining the goal of a simple structure. The stator and mover of the motor mimics the Halbach magnet array, with the magnet array enhancing the magnetic field on one side, thereby increasing the interaction force and efficiency between the stator and the mover. This type of magnet array also concentrates the magnetic field in one direction and reduces the surrounding magnetic force, thus reducing electromagnetic

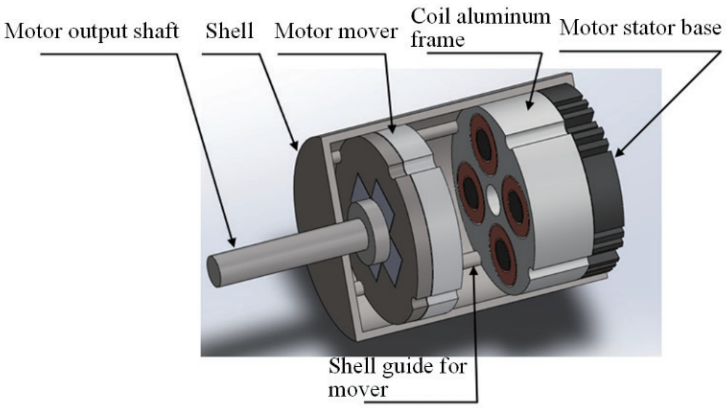

Fig. 1. (Color online) 3D preview of motor design.

interference in the vicinity. Since the magnet array forms N and S poles on the same side, the motor needs tracks or other ways to fix the direction of the magnets. Without proper fixation, the operation of the poles may lead to motor malfunction.

Figure 2 illustrates the structural design of the electric nail gun proposed in this paper. The construction of the nail gun is straightforward, consisting only of a stator, mover, track, nail, battery, control circuit, and safety rod. Figure 3 illustrates the control circuit of the electric nail gun. When the battery is connected, the capacitor begins charging. The linear motor is energized upon pressing the trigger switch, generating a magnetic field in the stator that drives the mover to propel the nail forward. The gun needle hits the nail and presses it into the workpiece, after which the mover returns to its original position via the return spring. If the safety lever and trigger switch are not pressed simultaneously, the electric nail gun will not take action. The magnetic orientation of the mover in the designed nail gun can be ensured by using slots machined into the casing or installing a slide rail. Furthermore, the reciprocating motion of the mover during operation also induces gas movement. The heat generated by the mover coils can be dissipated by drawing air through ventilation holes in the casing, facilitating heat diffusion. The control circuit utilizes voltage to control the activation and deactivation of the gate of the metal-oxide semiconductor field-effect transistor (MOSFET) without producing electrical sparks. The flyback diode releases energy stored in the stator when the circuit is turned off, protecting the circuit and preventing voltage surges.

2.1.1 Mover magnet geometry design

Considering that the internal cylinder of the nail gun in this study with a diameter of 50 mm has both forward and backward motion capabilities, the conventional bar-type magnet array is unsuitable for this design. Therefore, in the mover design in this study, the planar magnet arrangement is replaced with a circular arrangement, as shown in the enlarged view of the mover model in Fig. 4. We attempt to use magnets of different sizes with overlapping parallel and perpendicular magnetic sections. Notably, the magnets in front of the mover are cylindrical,

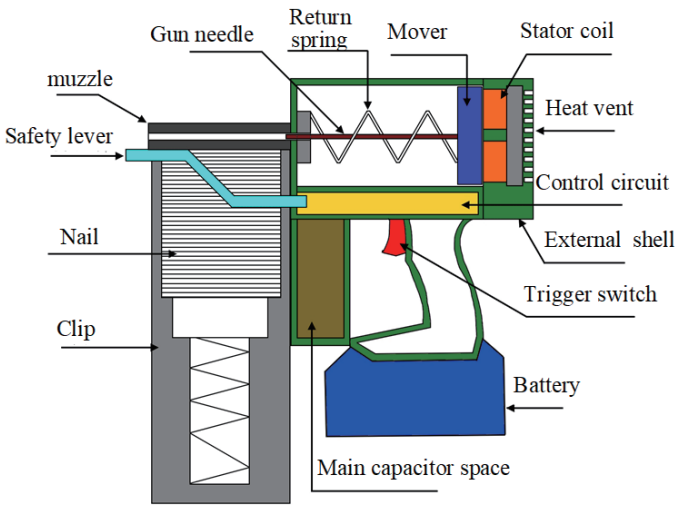

Fig. 2. (Color online) Schematic of electric nail gun structure.

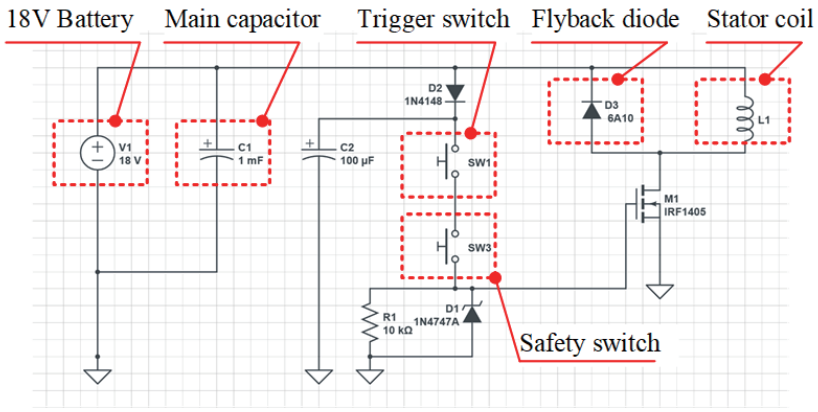

Fig. 3. (Color online) Electric nail gun control circuit diagram.

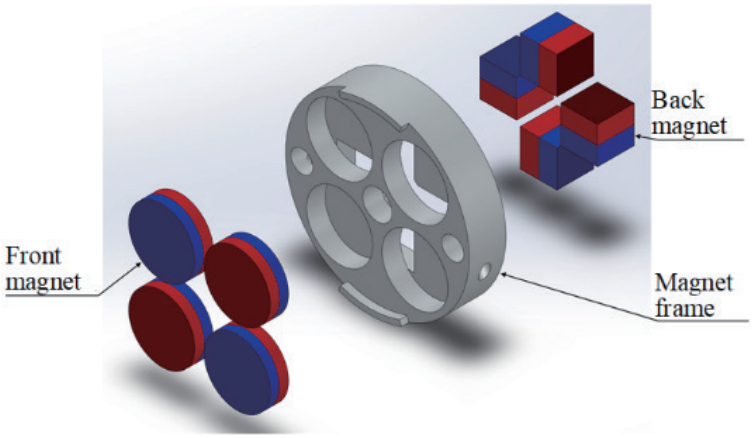

Fig. 4. (Color online) Enlarged view of mover model.

while those behind it are square. A cylindrical magnet at the front was chosen to match the action of the electrical coil. However, there are two reasons for using square magnets at the back. One is that the axial magnetized circular magnets are difficult to obtain, and the contact surfaces of the cylindrical magnets with axial magnetization do not fit well with the front magnets. The other is that the magnet must be replaced during the test experiment. Fixing the magnetic pole direction is difficult if cylindrical magnets are selected. Therefore, the dimensions of the magnets are designed considering the sizes available on the market. In Fig. 4 the red and blue colors represent the N and S poles of the magnets, respectively, which are illustrated in the schematic diagram of the mover's magnetic field distribution in Fig. 5. The symbols "⊙" and "×" represent the directions of the magnetic field pointing outward (N pole) and inward (S pole), respectively. Neodymium (NdFeB) magnets of grade ND-35 are used, with circular magnets in the front with dimensions of 18 × 5 (H) mm^2 and square magnets in the back with dimensions of 10 (L) × 10 (W) × 10 (H) mm^3.

Figure 6(a) shows the method of measuring the magnetic field of the mover using a Gauss meter of F.W. Bell 5180, produced by Johnson and Allen Ltd. Figure 6(b) shows that initially, only the four circular magnets on the front side were installed for measurement, with the N pole in the front and the S pole in the back. The peak magnetic fields on the front side were 2611.82

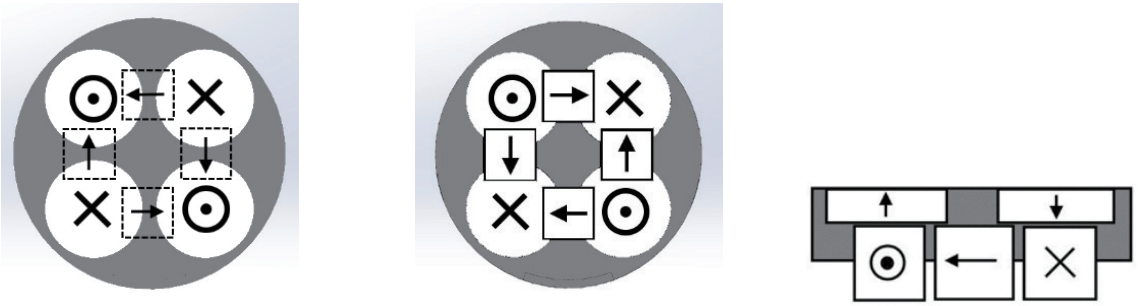

(a) (b) (c)

Fig. 5. (Color online) Illustration of mover magnet arrangement: (a) front view, (b) back view, and (c) side view.

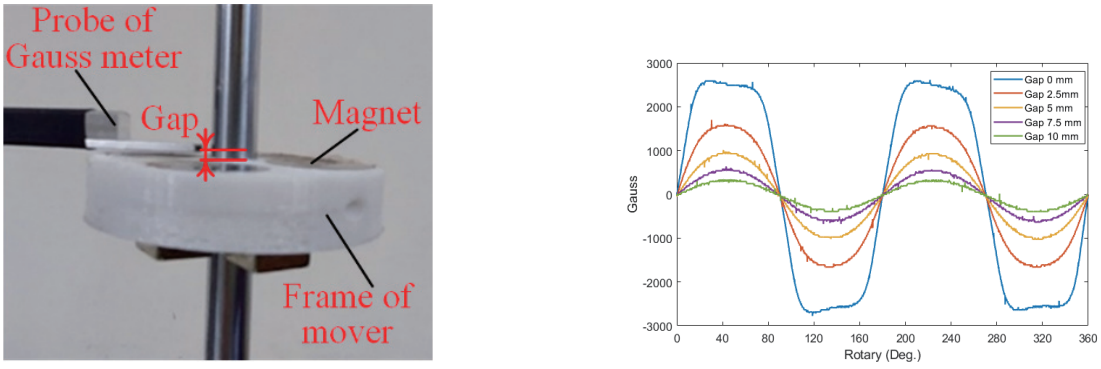

(a) (b)

Fig. 6. (Color online) Measurement of the magnetic field of mover magnet: (a) magnetic field measurement mechanism, (b) front side of nonmagnet array, (c) front side of magnet array, and (d) back side of magnet array.

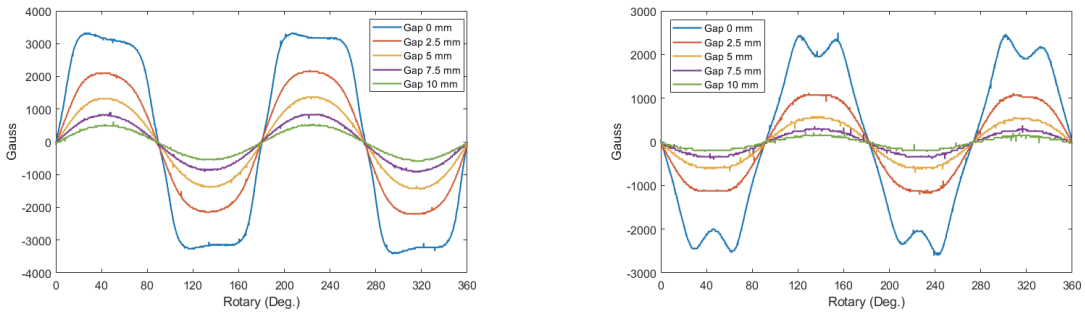

(c) (d)

Fig. 6. (Color online) (Continued) Measurement of the magnetic field of mover magnet: (a) magnetic field measurement mechanism, (b) front side of nonmagnet array, (c) front side of magnet array, and (d) back side of magnet array.

and −2776.03 Gauss. Upon installing the back magnets to form the magnet array, Fig. 6(c) shows that the peak magnatic fields of the front side after forming the magnet array were measured to be 3320.31 and −3433.84 Gauss, indicating that the magnetic field after forming the array was 1.27 times that before creating the array. Then, Fig. 6(d) illustrates that the peak magnetic fields of the back side after forming the magnet array were measured to be 2501.28 and −2607.67 Gauss. The measurement results indicate that the intensity of the front magnetic field is higher than that of the back magnatic field, and the back magnetic field is lower than the 2611.82 Gauss measured without the magnet array; therefore, the expected effect of the magnet array has been achieved. This method will be used in finite element analysis of the magnetic field to increase the front magnetic field and reduce the back magnetic field.

2.1.2 Stator magnetic field and geometric shape design

The magnetic force $\mathfrak{F}$ required to establish magnetic flux ($\varnothing$) in the magnetic circuit is defined as the magnetomotive force and is given by

$$\mathfrak{F} = N \cdot I \tag{1}$$

with units in ampere-turns. Note that N represents the number of turns in the coil, and I represents the current flowing through the coil (in amperes). By increasing either the number of turns or the current, we can enhance the electromagnetic force of the electromagnet. We adopt the 18 V power battery commonly used in hand tools as the design reference for power input. Under the premise of a fixed wire diameter, increasing the number of turns will increase the wire resistance and decrease the current. Furthermore, considering the restrictions of the piston inside the nail gun, the coil size is set to an outer diameter of 18 mm, an inner diameter of 10 mm, and a height of 15 mm. The diameter of the enameled wire is 0.4 mm, and the core diameter is 10 mm. The number of turns per layer and the wire length are calculated and used to calculate the coil resistance R as

$$R = \rho \cdot \frac{l}{A}, \tag{2}$$

where ρ is the resistivity (copper resistivity =1.72 × 10^{-8} Ω·m), l is the wire length (in meters), and A is the cross-sectional area of the wire (m^2). With enameled wire having a diameter of 0.4 mm, 370 turns can be ideally wound within the limit of the coil diameter of 18 mm. However, owing to the uneven tension in the handmade coil, the designed number of turns is reduced to 333 turns with a space of 0.8 mm reserved for the coil's outer diameter.

The material of the core affects the magnetic field of the electromagnet. Cores are used to increase the coil's magnetic flux to enhance the electromagnet's maximum power conversion. Core materials can include pure iron, wrought iron, low-carbon steel, or silicon steel sheets, with materials exhibiting higher permeability being preferable for the core. Generally, the relative permeability of cores ranges from 2000 to 6000. However, high-frequency magnetic field changes in motors can induce eddy currents in the core, resulting in iron loss. Using silicon steel sheets as the core reduces iron losses. These sheets are manufactured into thin laminations, and insulation layers are added between the metal layers to block the current flow between layers and minimize iron loss. The stator of the linear motor designed in this study uses DC electromagnets. Unlike conventional motors that operate at frequencies ranging from the order of 102 to 103 Hz, the operating frequency of the designed linear motor is primarily determined by the user's working speed. The hand-held nail gun construction speed is typically in the range of a few Hz, resulting in more minimal iron losses at lower motor frequencies.

Simulations of the motor base in the design revealed a minimal impact on the motor's magnetic circuit. Therefore, aluminum can be used for the motor base, and heat-dissipating fins can be incorporated to reduce the motor's temperature. Hence, choosing materials with high permeability for the core is preferable, and there is no need to stack silicon steel sheets. Instead, a single material for the core can be chosen, allowing for diverse material selection and simple manufacturing processes. Figure 7 depicts the structural design of the stator. However, in this study, the circular magnets on the front side are replaced with electromagnets, while permanent

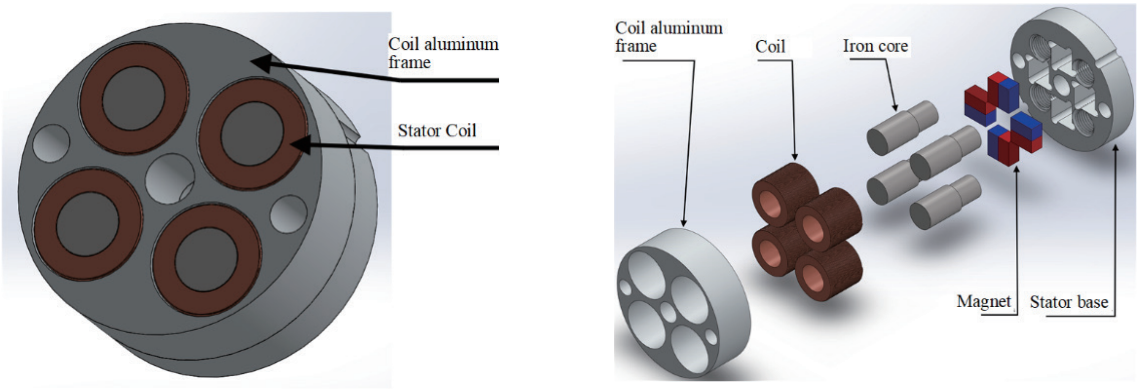

(a) (b)

Fig. 7. (Color online) Geometric design of stator model: (a) 3D schematic diagram of the stator and (b) enlarged view of the stator model.

magnets are maintained at the back as the motor does not require phase shifting. The magnetic field characteristics of electromagnets are similar to those of permanent magnets. Therefore, the design approach for the stator is that both electromagnets and permanent magnets are used to enhance the controllability of the stator's magnetic field. Finally, the stator model with a diameter of 50 mm and a thickness of 25 mm is created using SOLIDWORKS software.

Figure 8 illustrates the direction of the electromagnet and permanent magnet poles. Firstly, the core and the coil are combined to form an electromagnet, which is then integrated with the permanent magnet assembly on the base to constitute the stator assembly of the magnet array. Overlapping the coil and the permanent magnet helps to reduce the diameter of the motor, while embedding the core into the base facilitates heat dissipation, which is particularly advantageous for an aluminum base. The permanent magnets on the stator measure 10×10×5 mm and differ in size from the back magnets used on the mover. The stator magnets primarily generate the magnet array effect with minimal impact on the motor output. An aluminum frame for the coil protects it and facilinates heat dissipation. Once the remaining stator parts are completed, the aluminum frame is fitted. A thermally conductive adhesive is applied to the gap between the coil and the aluminum frame to enhance heat dissipation.

2.2 Simulation analysis of stator and mover magnetic fields

2.2.1 Mover magnetic field analysis

Simulation of the mover is relatively simple and quick, requiring only the correct settings of the magnet material and magnet direction for the simulation to proceed. The enlarged view of the mover model is depicted in Fig. 4. In this study, permanent magnets, specifically neodymium–iron–boron magnets with a grade of ND-35, are adopted for the mover. Within Altair Flux 3D, the corresponding parameters are defined in FLU_NDFE35. Figure 9 illustrates the simulated magnetic field intensity of the mover. The maximum front magnetic field intensity ranges from 1.15 to 1.24 T, with a lower magnetic field being observed in the region where the circular magnet is offset from the center. Additionally, noticeable color variations are observed

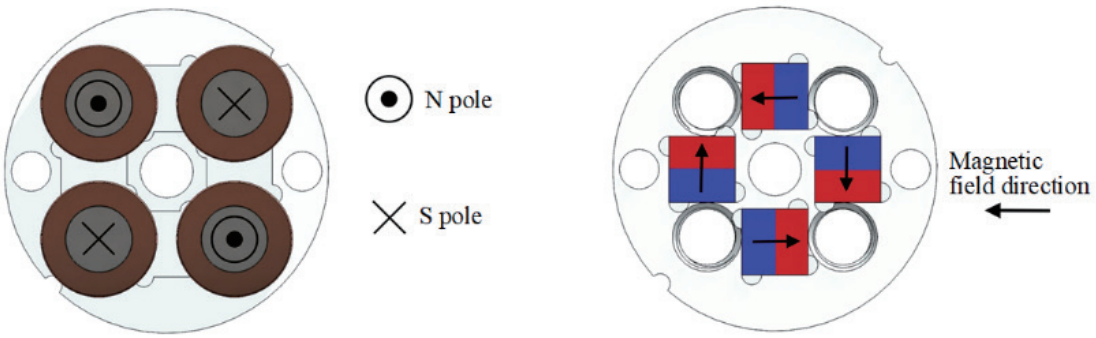

(a) (b)

Fig. 8. (Color online) Stator magnet directions: (a) electromagnet direction and (b) permanent magnet direction.

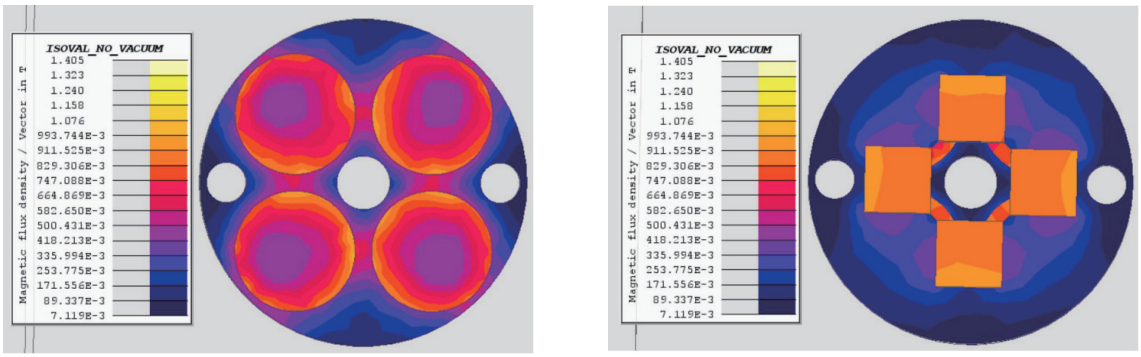

(a) (b)

Fig. 9. (Color online) Simulation results of mover's magnetic field intensity: (a) front view and (b) back view.

between the two sets of circular magnets, indicating the presence of magnetic fields between the magnets. The back magnetic field intensity is generally lower, remaining below 1 T. Similarly, color variations representing magnetic field intensity are observed between the square magnets, indicating the presence of magnetic fields between these magnets. Furthermore, Fig. 10 shows results of the mover's magnetic field direction analysis. Upon assembly into the magnet array, the frontal magnetic field forms two N poles and two S poles, totaling four poles. The back magnetic field consists of six N poles and six S poles, totaling 12 poles, because there are four poles behind the front magnets and eight poles from the flat back magnets.

Figure 11 presents the results of the magnetic flux analysis for the mover. In Fig. 11(a), the yellow regions represent the magnets. The magnetic flux lines display an arc shape on the frontal side, where flux lines emitted from the N pole tend to converge towards and enter the adjacent S poles. Figure 11(b) depicts the side view of the magnetic flux lines with directional indicators. Similarly, flux lines originate from the N pole of one magnet and enter the S pole of the adjacent magnet. Subsequently, the flux lines pass through the back magnets before returning to the original magnet. The flux lines on the front side form an arc shape, with the highest point of flux concentration observed at the junction between the front and back magnets. Additionally, the magnetic flux outside the area of the picture in Fig. 11(b) is relatively sparse, with the magnetic field being concentrated in the direction corresponding to the magnet array.

2.2.2 Stator magnetic field analysis

In this study, the stator core material is 35CS550_DC from China Steel Corporation, Taiwan, the parameters of which can be easily set using the internal database of Altair Flux 3D software. The stator core has the dimensions of 15 mm in height and 10 mm in diameter, with a maximum outer winding diameter of 18 mm. With a wound coil of 333 turns, the measured coil resistance is 2.2 Ω. As illustrated in Fig. 7, the stator comprises four winding poles. To increase current flow, we adopt a configuration of four coils connected in parallel to reduce resistance. Consequently, the resistance after the parallel connection is 0.55 Ω. If an 18 V battery provides the power supply voltage, applying Ohm's law yields an estimate of 32.72 A for the current

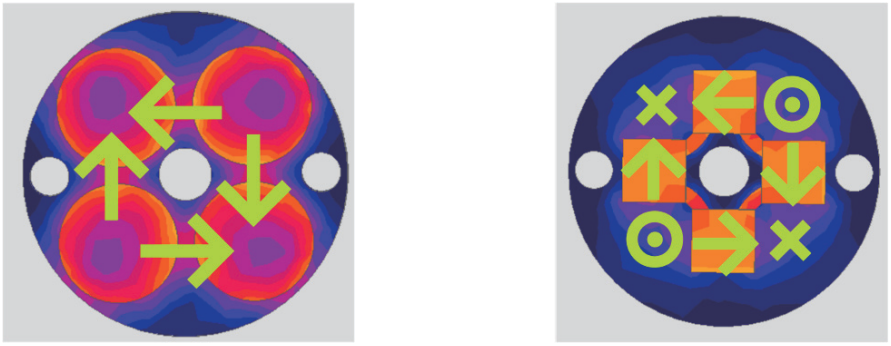

(a) (b)

Fig. 10. (Color online) Analysis results of the magnetic field direction of the mover: (a) front view and (b) back view.

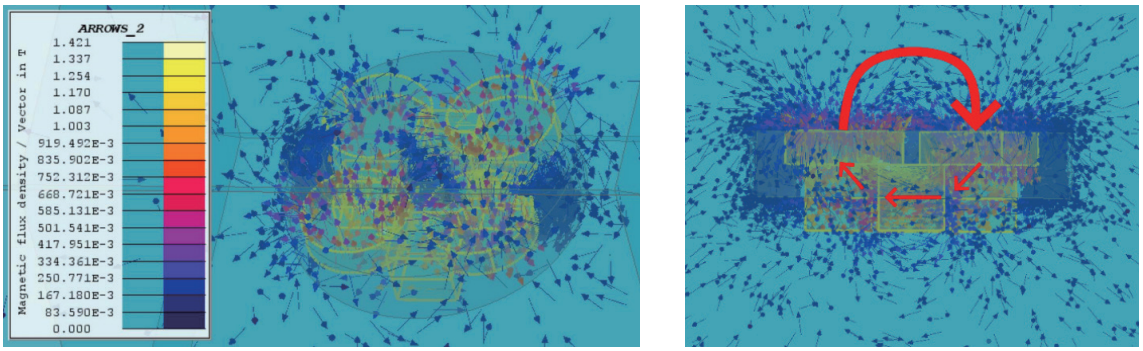

(a) (b)

Fig. 11. (Color online) Results of mover magnetic flux analysis: (a) front view and (b) side view.

passing through the coil. However, considering potential errors in the actual resistance of coil production, the input current for simulation is set at a conservative value of 30 A. Figure 12 illustrates the simulation results with a stator coil input current of 30 A. The results show that the front magnetic field is more substantial, having a magnetic field intensity of 2.2 T at the top of the electromagnet, approximately 1.8 times higher than 1.2 T on the back side, aligning with the characteristics of the magnet array.

Figure 13 depicts the stator's magnetic flux analysis results, with the yellow regions representing the magnetic core and permanent magnets. Figure 13(a) shows the Flux 3D analysis results of magnetic flux distribution encompassing the surrounding air region. The colors of the arrows indicate the magnetic field strength, with brighter colors signifying stronger magnetic fields and darker colors indicating weaker ones. However, owing to limitations in Flux 3D's display of magnetic flux line orientations, Fig. 13(b) shows manual labels; red arrows denote the direction of the magnetic field, with different shades of arrow colors distinguishing between flux lines from the front and back magnets. The stator's assembled magnet array forms four poles on the front side, consisting of two sets of N poles and two sets of S poles. Figure 13(c)

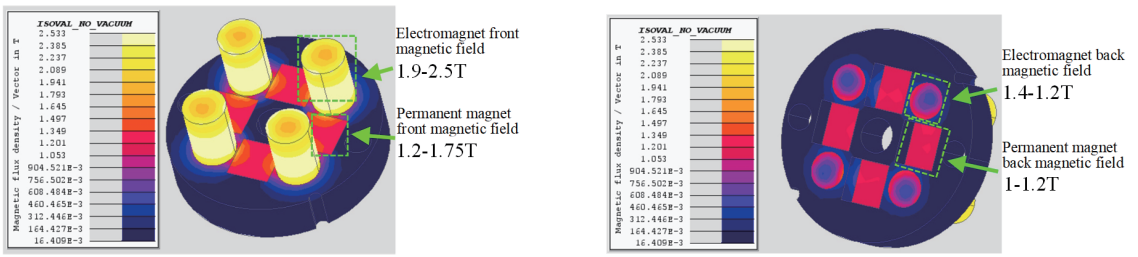

(a) (b)

Fig. 12. (Color online) Magnetic field analysis results of the stator: (a) front view and (b) back view.

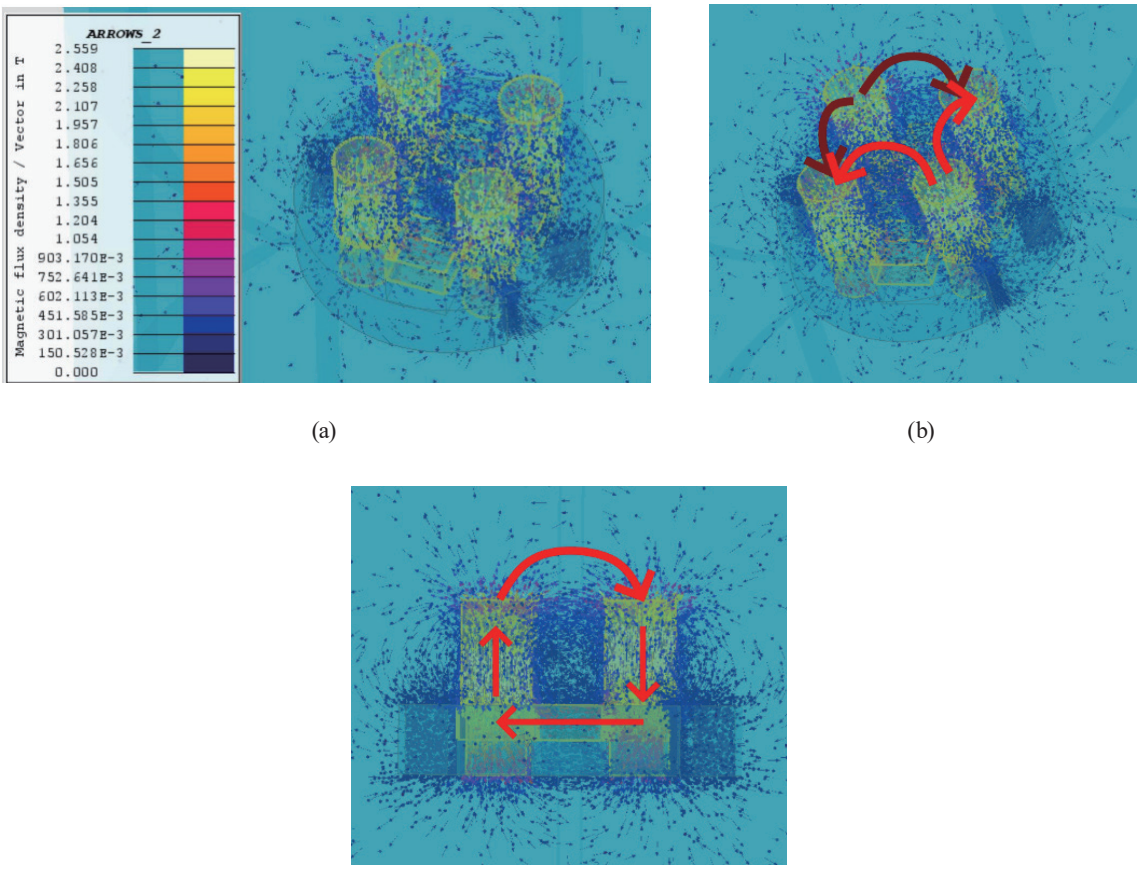

(a) (b)

(c)

Fig. 13. (Color online) Stator magnetic field line distribution: (a) magnetic field line simulation results, (b) schematic diagram of magnetic field direction, and (c) schematic diagram of side magnetic field line.

shows the side view of the stator's magnetic flux analysis results, with brighter colored arrows indicating higher magnetic field intensities at the top and lighter colored arrows indicating lower magnetic field intensities at the back. Additionally, it is observed that the magnetic flux outside the picture area in Fig. 13(c) is also relatively sparse, indicating that the magnetic field is concentrated in the specified direction of the magnet array.

2.2.3 Simulation of linear motor force

The model is imported into the Flux 3D analysis software after assembling the stator and mover in SOLIDWORKS. Subsequently, the N pole of the mover is aligned with the N pole of the stator. The model does not include a track, and a 1 mm gap is maintained between the mover and stator, to accommodate the magnetic cover made of nonmagnetic material used in practical implementation. Figure 14 illustrates the magnetic field simulation analysis results of the assembled linear motors. The surface magnetic field matches the results of the previous simulation. Figure 14(b) shows the magnetic field distribution viewed from the side. The magnetic force is highest in the gap between the movers, where repulsion occurs because of the similar poles. Outside the area outlined in Fig. 14(b), the magnetic flux lines around the motor perimeter are sparse, consistent with the design requirements. Reducing the magnetic field outside can minimize electromagnetic interference.

The built-in force calculation feature in the Altair Flux 3D software is used to display the force acting on the front magnet of the mover as the recorded object. Simulations with coil input currents ranging from 0 to 30 A are carried out; the force exerted on the mover is shown in Fig. 15(a). From the graph, it can be observed that a current input of 30 A yields a force of 246.6 N.

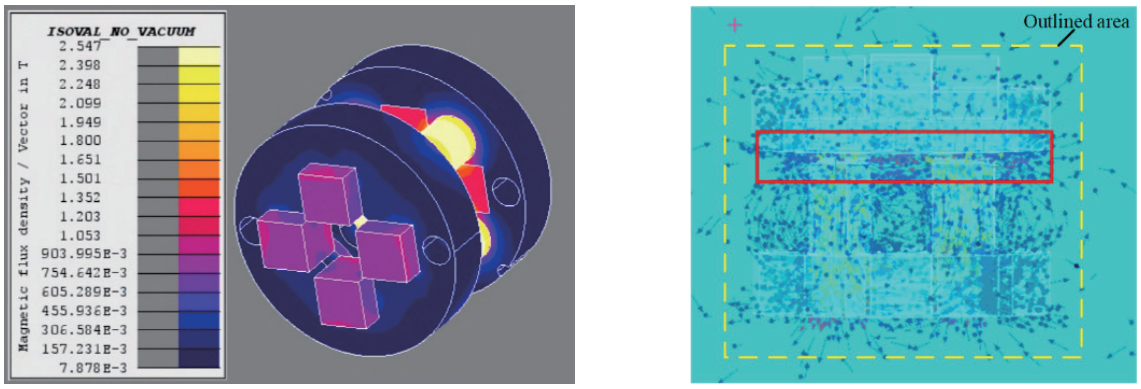

(a) (b)

Fig. 14. (Color online) Results of linear motor magnetic field simulation analysis: (a) front view from the mover and (b) magnetic field distribution viewed from the side.

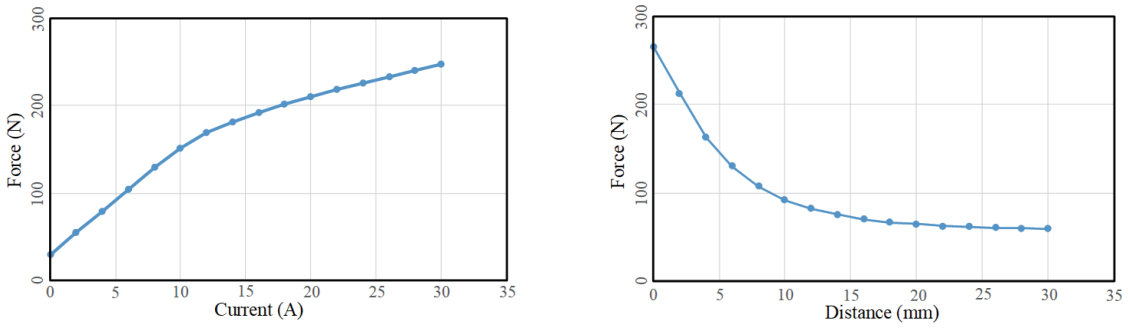

(a) (b)

Fig. 15. (Color online) Relationship between stator and dynamic force: (a) current and force and (b) distance and force.

When the input current is 6 A, the target of 100 N is achieved. The stator core material used in the simulation is 35CS550_DC, a nonlinear saturable material, from China Steel Corporation, Taiwan. The force varies nonlinearly with the current. As the current increases and approaches the magnetic saturation of the core material, the growth of the magnetic field slows down. Figure 15(b) illustrates the relationship between force and distance as the mover moves away from the stator. It can be observed that the force gradually decreases as the mover moves away from the stator.

3. Experimental Results and Discussion

Figure 16 shows the setup of the linear motor test. Figure 16(a) is a schematic of the setup for measuring the force exerted by the electric nail gun. The stator is fixed and installed inside the gun body, while the mover and motor firing pin are fixed together and can move forward and backward inside the cylindrical gun body. The stator current is measured using a PROVA 15 current probe. In the 30 A range, the probe outputs 10 $mV{\cdot}A^{-1}$, which can be displayed on an oscilloscope. Figure 16(b) shows the actual test setup. The force at the measuring point is measured using an HP-100 digital torque meter, which indirectly measures torque using the leverage principle. HP-100 is designed for torque measurement in rotary hand tools. Additionally, to control the switching time of the MOSFET during experiments and reduce measurement variations, an Arduino Nano is used as a controller to regulate the power switch-on time. However, the General-purpose input/output of Arduino Nano can only output a voltage of 5 V and cannot directly open the MOSFET. Therefore, a photocoupler-integrated circuit, PC817, is added to the gate circuit to allow Arduino Nano to control a higher driving voltage for the MOSFET.

Figure 17 shows the results of mechanical work measured with power-on times from 1 to 50 ms. The measurement indicates that the linear motor reaches its maximum output of 62.1 N at a current input of 5.62 A. This output is significantly lower than the Flux 3D simulated value of

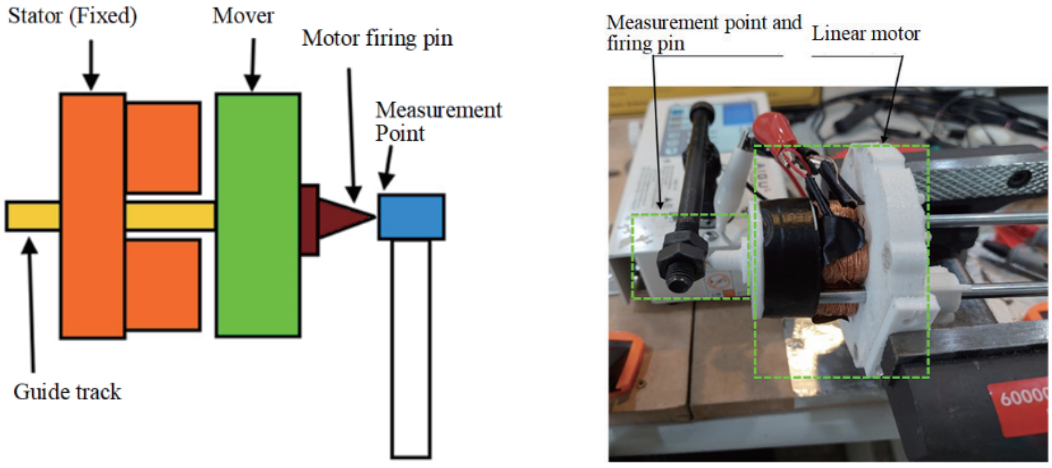

Fig. 16. (Color online) Experimental test setup: (a) schematic diagram of the motor test and (b) actual test setup.

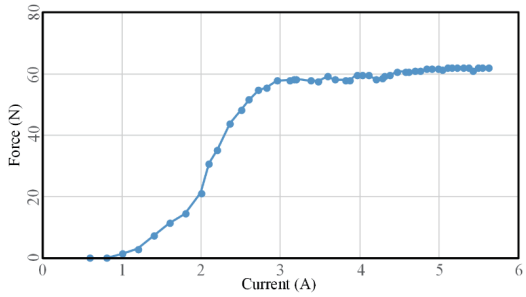

Fig. 17. (Color online) Experimental results of current input and force.

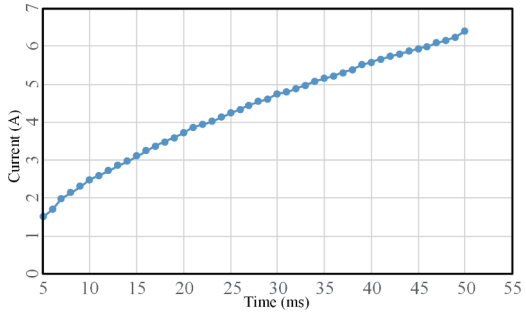

Fig. 18. (Color online) Relationship between switch conduction time and current.

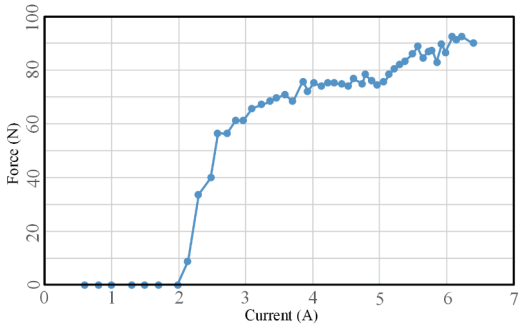

Fig. 19. (Color online) Relationship between current and force with the firing pin held at a distance of 15 mm from the measurement point.

104 N at 6 A. This difference is attributed to the use of an inferior stator core material. The permeability of the steel screws used to make the core is much lower than that of the silicon steel sheets used in the simulation, causing magnetic saturation of the core. This discrepancy arises because the stator core material used in the experiment differs from the 35CS550_DC stator core material (China Steel Corporation, Taiwan) used in the simulation and exhibits poorer performance. However, from the graph, it can be observed that the core made of screws closely matches the simulation results when the input current is 3 A, as the core has not yet reached magnetic saturation at this point.

Figure 18 illustrates the relationship between the conduction time of the switch and the current data. From Fig. 18, it is observable that there exists a direct proportionality between the conduction time and the input current. By controlling the conduction time of the switch, we can regulate the current input to the coil. Additionally, the lithium battery's voltage is not fixed; when fully charged, the voltage is 20 V and gradually decreases as the battery discharges. Consequently, at the same conduction time, the current varies to a certain degree owing to fluctuations in battery voltage. Furthermore, during the experimental process, it was noted that maintaining a distance between the plunger and the measuring point resulted in a higher output power than in the case of direct contact. Figure 19 shows the experimental results of controlling the coil's input current by manipulating the switch time while maintaining a test distance of 15

mm. From the test results, it was determined that the average maximum output force was 90 N, which is significantly higher than the 62 N achieved with direct contact. For instance, the output forces of the noncontact and direct contact scenarios at an input current of approximately 5.5 A were measured to be 88.7 N and 62 N, respectively. This implies that the output forces obtained while maintaining a 15 mm distance during measurement are 1.43 times higher than those obtained with direct contact.

4. Conclusions

In this paper, we showed the linear motor verification design applied to an electrical nail gun using a Halbach magnetic array. From the results of the simulation analysis and practical experimental measurements, the following conclusions can be drawn.

(a) Magnetic array technology can be applied to the design of linear motors for electric nail guns. The linear motors produced can achieve a maximum average output of 90 N with a 15 mm spacing between the wall and the nail, even when using inferior iron core materials. This output power matches that of gas-powered concrete nail guns. In direct contact tests, an output power of 60 N was achieved, which is suitable for electric nail guns requiring a lower power output. Since this motor does not require energy storage, its operating speed surpasses those of existing spring-based electric nail guns, and its output power exceeds those of coil-based nail guns.

(b) Magnetic arrays can be formed using different magnet sizes and geometries. Overlapping magnetic portions also enhances the unidirectional magnetic field of the magnetic array, although the enhancement effect is lower than that of the original flat arrangement.

(c) Electromagnets can be combined with permanent magnets to form magnetic arrays. Permanent magnets have fixed magnetic poles, making them unsuitable for motors requiring variable phases. However, they can be used in applications where the current direction is fixed, elimnating the need for coil usage, thereby reducing motor manufacturing difficulty and copper losses that generate heat.

(d) From the simulation results, it can be observed that the motor's generated magnetic field is concentrated internally, resulting in minimal electromagnetic interference from the surrounding area. This can reduce the need for magnetic shielding materials. The motor stator pushes out the mover before reaching a high current.

In addition, the results also suggest the need for a delayed firing mechanism that delays the movement of the mover by a few milliseconds so as to maintain its position until the designated current is reached, enabing mover movement at maximum force. For the delayed firing mechanism, one can refer to the delayed unlocking mechanism in firearms as a reference. In the future, the design of a linear motor for application to an electrical nail gun will be further optimized using motor-specific cores and materials by finite element analysis using the software Altair Flux 3D and experiments to enhance the output power and controllability.

Acknowledgments

This research was partially supported by the National Science and Technology Council of the Republic of China under contract NSTC 112-2221-E-230-002.

References

1 What Type of Nail Gun Is Best for Framing: https://home.howstuffworks.com/type-of-nail-gun-install-floor-studs.htm (accessed May 2024).
2 Global Power Tools Market-2023-2030: https://www.gii.tw/report/dmin1247429-global-power-tools-market.html (accessed May 2024).
3 Z. Ahmadabadi, F. Laville, and R. Guilbault: Appl. Acoust. **114** (2016) 191. https://doi.org/10.1016/j.apacoust.2016.07.030
4 M. Vincent, T. Padois, M.-A. Gaudreau, T. Dupont, and P. Marcotte: Proceedings. **86** (2023) 20. https://doi.org/10.3390/proceedings2023086020
5 V. Jayakumar, J. Kim, and E. Zechmann: Noise Control Eng. J. **63** (2015) 15. https://doi.org/10.3397/1/376315
6 Z. Ahmadabadi, R. Guibault, and F. Laville: Math. Comput. Modell. Dyn. Syst. **25** (2019) 195. https://doi.org/10.1109/ICMRA51221.2020.9398345
7 G. Zhenghao, W. Siyuan, and W. Tao: 2020 3rd Int. Conf. Mechatronics, Robotics and Automation (ICMRA, 2000) 1–5.
8 L. Selçuk and K. Kayabali: Eng. Geol. **195** (2015) 164. https://doi.org/10.1016/j.enggeo.2015.06.014
9 The Electric Nail Gun Lacks Power: https://www.ces-transaction.com/html1/report/2004/546-1.htm (accessed February 2024).
10 DCN890P2, Cordless Concrete Nailer Kit: https://www.dewalt.com/product/dcn890p2/20v-max-xr-cordless-concrete-nailer-kit?tid= (accessed May 2024).
11 H. Wang, X. Liu, C. Sun, and H. Li: J. Appl. Sci. Technol. **26** (2023) 1585. http://doi.org/10.6180/jase.202311_26(11).0008
12 C. Chen, R. Wu, B. Tsai, and C. Hsu: Microsyst. Technol. **27** (2021) 1019. https://doi.org/10.1007/s00542-018-4007-y
13 J. Mallinson: IEEE Trans. Magn. **9** (1973) 67. https://doi.org//10.1109/TMAG.1973.1067714
14 B. Reutzsch and W. Schinkoethe: 2013 Innovative Small Drives and Micro-Motor Systems; 9 GMM/ETG Symp. (IEEE, 2013) 1.
15 S. Wu, S. Cui, and W. Zhao: IEEE Trans. Plasma Sci. **43** (2015) 1377. https://doi.org/10.1109/TPS.2015.2404139
16 T. Gogo, C. Alexandru, and D. Zhu: 2021 IEEE 20th Int. Conf. Micro and Nanotechnology for Power Generation and Energy Conversion Applications (PowerMEMS, 2021) 52.
17 K. P. Lijesh and H. Hirani: Prog. Electromagn. Res. C **56** (2015) 173. https://doi.org/10.1109/TMAG.1973.1067714
18 L. Duan, H. Lu, C. Zhao, and H. Shen: 2020 IEEE Int. Conf. Artificial Intelligence and Computer Applications (ICAICA, 2020) 994–998.
19 T. Itasaka, Y. Ishiguro, K. Shinozaki, J. Watanabe, D. Wakamatsu, A. Ito, and H. Suzuki: 2019 12th Int. Symp. Linear Drives for Industry Applications (LDIA, 2019) 1.
20 N. Morimura, H. Suzuki, and M. Morishita: 2018 21st Int. Conf. Electrical Machines and Systems (ICEMS, 2018), 27.